Geophys. J. Int. (2006) **165,** 931–942 doi: 10.1111/j.1365-246X.2006.02973.x

Automated *SKS* splitting and upper-mantle anisotropy beneath Canadian seismic stations

M. S. Evans,[1,*] J.-M. Kendall[2] and R. J. Willemann[3]

[1] *School of Earth and Environment, University of Leeds, Leeds,* LS2 9JT, *UK*
[2] *Department of Earth Sciences, University of Bristol, Wills Memorial Building, Queens Road, Bristol,* BS8 *1RJ, UK*
[3] *IRIS, suite* 800, 1200 *New York Avenue, NW, Washington DC* 20005, *USA*

Accepted 2006 February 10. Received 2005 December 12; in original form 2005 July 13

SUMMARY

We have developed an automated method for measuring shear wave splitting and applied it to *SKS* phases recorded at permanent broad-band stations in Canada. Our method performs two measurements, one seeking to minimize the energy on the transverse component, the other minimizing the smaller of two eigenvalues calculated from the covariance matrix of particle motion. A short-term-average/long-term-average (STA/LTA) phase picker is used to identify *SKS* arrivals and successive splitting measurements are made on incrementally larger windows around the *SKS* arrival. The final result is derived from the longest series of windows over which the splitting parameters remain constant. In this study we have processed over 20 000 station/event combinations from 34 stations and 1540 events. Roughly 2 per cent of the data produce reliable estimates of splitting, due to the stringent quality controls applied. We find good correlation between our results and previously published results from the same stations. At some stations we find significant differences in results between the two methods, an observation that has been verified using manual measurements. In each case, eigenvalue derived measurements are consistent with a single layer of anisotropy but transverse-energy derived results require a more complex interpretation. This discrepancy can be explained by misalignment of horizontal components. Tests with synthetic seismograms show that component misalignment can lead to false interpretations of multilayer or dipping anisotropy using the transverse-energy method. The quality of results at individual stations is variable, being influenced both by the volume of available data (determined by station deployment date and the distribution of natural seismicity), and the performance of the STA/LTA picker used to define the start of the *SKS* window. We compare the orientation of the inferred anisotropy at each station with local tectonic features and directions of absolute plate motion (APM); there is no consistent correlation. Many stations give results that agree with both, while some agree better with local geology and others agree better with APM directions. Results are available through a dedicated website and provide a potential aid to other studies of anisotropy in the deep Earth.

Key words: anisotropy, Canada, shear wave splitting.

1 INTRODUCTION

Measurements of shear wave splitting provide one of the most robust pieces of evidence of wave propagation through anisotropic media. The analysis of splitting in seismic phases that transit the Earth's core (e.g. *SKS*) is a now routine tool for studying upper-mantle anisotropy (Silver & Chan 1991; Vinnik *et al.* 1989). Such analyses are normally performed manually and are guided to some degree by human intuition. The anisotropy beneath a seismic station is conventionally characterized by a dozen or so measurements, (e.g. Barruol & Hoffman 1999).

However, the amount of data available for analysis is increasing dramatically as the age and size of permanent networks get larger (Butler *et al.* 2004). Furthermore, temporary networks are now routinely comprised of over 100 stations. For example, USArray, a moving network of 400 broad-band instruments, will blanket the United States in seismic stations for 18-month temporary deployments (Levander *et al.* 1999). With such data sets manual measurements of *SKS* splitting become too time consuming. There is also

*Now at: AWE Blacknest, Brimpton, Reading, Berkshire, RG7 4RS, UK. E-mail: matthew@blacknest.gov.uk

a need for a consistent approach to measuring splitting at a station; in the past there have been inconsistencies in results reported by different authors for the same station. Hence, there is a need for an automated methodology for estimating shear wave splitting. Here we present such a methodology for *SKS* splitting and apply it to broad-band seismic stations in Canada.

When investigating *SKS* splitting, most waveforms will not yield reliable results for a variety of reasons. Event magnitude, *S*-wave radiation pattern, epicentral distance and station noise all influence the clarity of *SKS* signals. Unfortunately, the definition of a good splitting measurement is subjective, and results that would be dismissed by one researcher as unreliable may well be acceptable to another. This problem is only exacerbated by the use of different measurement and error estimation methodologies; subtle differences can have significant effects on the interpretation of splitting results. Review papers, (e.g. Silver 1996) often compile results from various authors, but the issue of differing methodologies is not usually addressed. One of the aims of our work is to ultimately provide a comprehensive global set of splitting measurements for use by the wider academic community. For example, knowledge of near-station splitting is required to investigate anisotropy in the deeper Earth (Wookey *et al.* 2005).

By developing an automated method for measuring shear wave splitting we are able to process a data set far larger than would otherwise be possible and with a consistency that is difficult with manual measurements. For comparative purposes, the landmark paper of Silver & Chan (1991) was based on measurements from 49 events recorded at 21 stations, of which only 62 *SKS* or *SKKS* phases were suitable for splitting measurements. In this report we present results from 1540 events recorded at 34 stations (shown in Fig. 1), which returns over 20 000 suitable station/event combinations. We compare these results with manual measurements performed on data from a subset of these stations and also with previously published work by other authors.

The data we analyse come from permanent stations of the Canadian National Seismic Network (CNSN) and the IRIS/IDA network (Fig. 1). These stations cover a remarkably diverse range of tectonic settings and, as such, measurements of *SKS* splitting at these stations offer insights into the nature of mantle deformation in various tectonic environments. Central to this lies the question of to what degree mantle anisotropy reflects active and past deformation processes (e.g. Silver 1996). It is possible that more than one domain of anisotropy lies beneath a station. Significant depth-dependent variations in anisotropy can be revealed by splitting results that vary systematically with the incoming azimuthal direction (backazimuth) of the *SKS* phase (Savage & Silver 1993). Therefore, confidently estimating multilayer anisotropy requires many measurements from a wide range of backazimuths.

2 THEORY

A planar *S* wave entering a weakly anisotropic media will split into two independent and perpendicularly polarized waveforms that will travel along the same ray path but separate with time. The orientations of the fast and slow shear waves are controlled by the symmetry or principle axes of the anisotropy. The resultant shear wave splitting can be described by the polarization direction of the first arriving *S* wave, ϕ, and the lag time, δt, between the two waves. Diagnostics of such splitting include *S*-wave energy recorded in the direction perpendicular to the initial *S*-wave polarization and elliptical *S*-wave particle motion. Ando & Ishikawa (1982) first used such splitting observations in vertically travelling phases to infer upper-mantle anisotropy beneath Japan. Vinnik *et al.* (1984) were the first to use observations of shear wave splitting in teleseismic core-transiting phases (e.g. *SKS*, *SKKS*).

Core phases like *SKS* become radially polarized emerging from the core–mantle boundary due to the *P*–*S* conversion, so any detected splitting can be constrained to the receiver side of the ray path. Their steep incidence angles and Fresnel-zone based arguments constrain the inferred anisotropy to the upper-mantle region beneath the station, assuming horizontal polarization directions (Alsina & Sneider 1995).

If only one anisotropic layer is encountered with horizontal fast and slow polarization directions, ϕ and δt values will remain constant with varying backazimuth, except where this corresponds to either of these principal axes. Here, the effect of the anisotropy

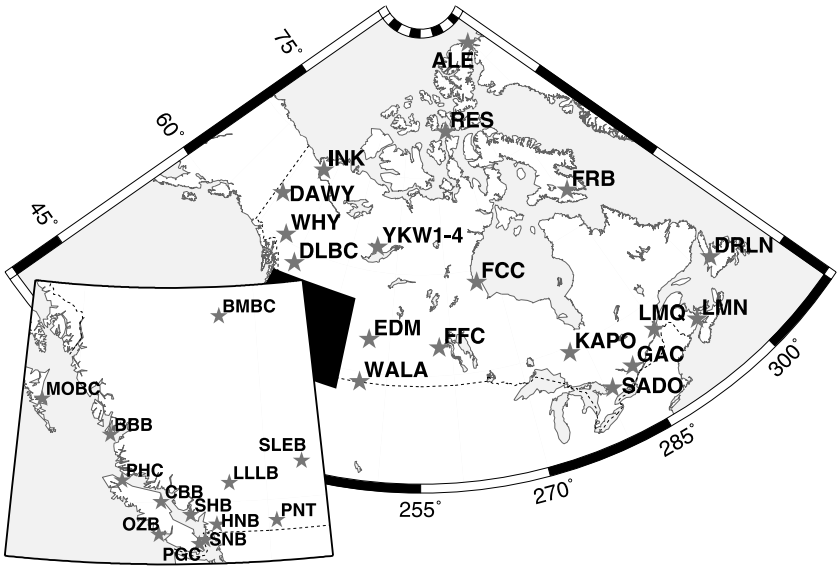

Figure 1. Canadian seismic stations used in this study. Stations are part of the CNSN, except ALE and FFC, which are operated by the IRIS/IDA—GSN network. Inset shows detail of station locations in British Columbia.

will be to increase or decrease the traveltime residual of the wave accordingly. With the incoming wave remaining polarized in the backazimuth and no energy on the transverse component, ϕ values generally match either of the principal axes and δt values remain unconstrained. Multiple layers of anisotropy or inclined symmetry axes result in systematic variations of ϕ and δt with backazimuth (e.g. Plomerova *et al.* 1996; Sileny & Plomerova 1996; Silver & Savage 1994).

3 METHOD

Measurements were performed on 34 three-component broad-band stations within Canada, 32 stations from the CNSN and 2 stations from the IRIS/IDA (II) network (see Fig. 1). These data are archived at the Canadian National Data Center (CNDC) and IRIS Data Management Center (IRIS DMC), respectively. For comparison, manual measurements were performed at ten of these stations using data from events between 1994 and 1998 inclusively. We searched the ISC catalogue to identify suitable events ($M_W \geq 5.8$) and then calculated the distance to each station. Station/event combinations outside a search window of 90° and 130° degrees were discarded. The lower limit ensures that the *SKS* phase is isolated from other potentially contaminating phases such as the direct *S* wave or *ScS*, while the upper limit prevents wasting processing time on more distant events where the *SKS* phase is normally too weak to provide clear measurements. The arrival time of the *SKS* phase was then predicted using the IASP91 earth model (Kennett & Engdahl 1991) and a suitable request window defined. A data request was then composed in an appropriate format (e.g. AutoDRM, NetDC or BreqFAST) and sent to the corresponding data centre. These data requests are then processed by the data centres, who subsequently send e-mail notification messages once the data become available. These files are then passed to our automated splitting software. This retrieval process is outlined in Fig. 2.

We then apply a short-term-average/long-term-average (STA/LTA) picker to more accurately identify the phase onset, and to discard waveforms with no clear *SKS* phase. This is performed on the radial component using a picking algorithm developed by Earle & Shearer (1994). The algorithm was initially developed to identify higher frequency *P* phases, so we have altered the suggested parameters to a combination better suited to identifying *SKS* phases. Our selection of picking parameters was chosen to be biased towards minimizing false negative results (where a good *SKS* signal is missed), as we have confidence that our quality control (QC) methods, discussed later, will identify the majority of false positives (where an *SKS* pick is unjustified). In order to prevent the picking of other phases we only accept picks within 12 s of the predicted arrival time. We define the window start at 5 s before the STA/LTA pick. We then filter the data, using a second order zero-phase bandpass Butterworth filter, with corner frequencies at 0.01 and 0.3 Hz.

Our automated system then performs two independent measurements using the eigenvalue and transverse energy methods described in Silver & Chan (1991). The eigenvalue method grid searches over ϕ and δt values for a combination that best linearize the particle motion or, in other words, minimize the smaller eigenvalue of the covariance matrix. The transverse energy method identifies parameters that minimize the energy on the transverse component. Both sets of results are presented here, to ensure compatibility with other work and because we have found inconsistencies between the two methods at some stations. We calculate two 1σ error estimates for each measurement method, one based on the inverse F-test (Silver & Chan 1991), and the other based on a bootstrapping technique (Sandvol & Hearn 1994) (see references for methodology). In this paper we use the Silver & Chan (1991) error estimates to ease comparisons with other already published work. Both error estimates are available through the website described below. Fig. 3 shows an example of a splitting measurement on an *SKS* arrival at the station WALA. After choosing the best splitting parameters and making the splitting correction, the *SKS* signal is removed from the transverse component and the particle motion is linearized.

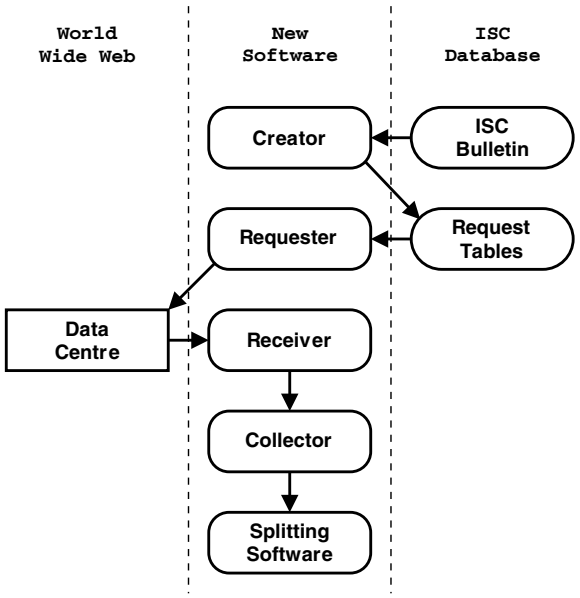

Figure 2. Simplified schema of the waveform retrieval process. The creator program identifies suitable data and makes entries into the database. The requestor program identifies these new entries and composes e-mail requests to the external data centres. Replies are sent to an e-mail address, which pipes the text to the receiver program where they are archived as individual files. These are processed by the collector, which identifies and retrieves the new waveform data via FTP. These waveforms are then converted to a common format and passed to the splitting software.

The most suitable window end time is found by performing successive measurements on incrementally larger time windows. Within this set of values, we find the longest series of measurements over which both ϕ and δt remain constant and define our window end to be at the centre of this series (see Fig. 4). An image is then generated to record information that may be useful for manually reviewing measurements. These are stored as GIF files on the ISC web server (http://www.isc.ac.uk/SKS) and can be accessed by users for manual review of data when using the web interface.

This style of automation, with station/event pairs processed sequentially and only the parametric data archived in the database, does not suit other splitting methods that process data from multiple events simultaneously such as the multichannel analysis of Chevrot (2000). It is therefore not implemented in this study.

The biggest challenge in automating shear wave splitting analysis has been developing a QC system, as defining what is a good measurement is essentially subjective. We perform five individual QC checks, summarized in Table 1, each hereafter identified by a letter code. 'A' and 'L' methods define the upper threshold for the errors calculated for polarization angle and lag time, respectively. They are, therefore, dependent on the error estimation method used. The 'T' method defines the maximum value for δt. In our measurements

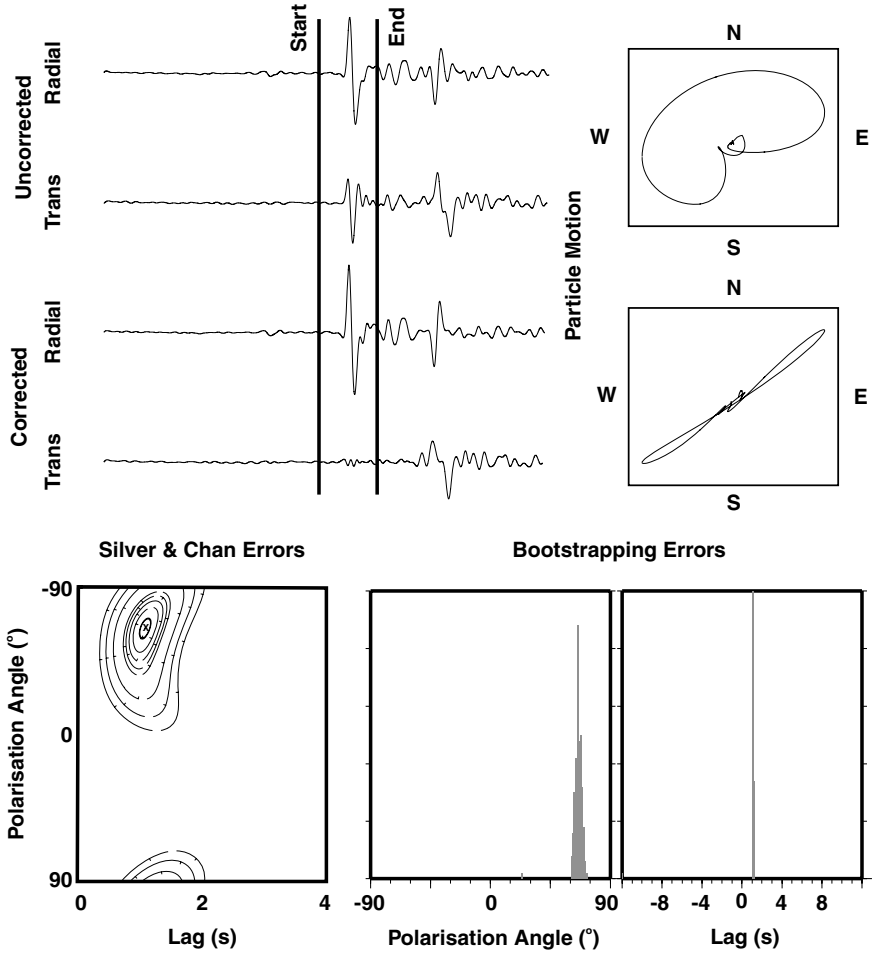

Figure 3. Example manual splitting measurement recorded at station WALA, from an event off New Britain (4.543 S, 154.8875 E, Date: 1996-05-02 13:34, Depth: 490 km). In the top left corner are four waveforms, the top two showing the radial and transverse components of the incoming split *SKS* phase, the bottom two showing the waveforms after they have been corrected for splitting. In the top right corner are the corresponding particle motion plots oriented north–south/east–west. The bottom left corner shows confidence intervals associated with the measurement calculated using the method of Silver & Chan (1991). The bottom right corner shows histograms calculated using the bootstrapping method of Sandvol & Hearn (1994).

we grid searched with δt values up to 12 s. From experience with manual measurements, we have found that for excessively noisy data, δt values tend to drift towards the upper limit of the search window, whatever that may be. By allowing these values to drift so high, well beyond the presumed plausible effects of splitting, we can easily identify and discard these values by setting the 'T' threshold to a more realistic value. The 'O' and 'C' methods measure the linearity of the particle motion. The corresponding values are defined as the ratio of the two eigenvalues of the covariance matrix (min/max) and so can range from 0 (perfectly linear) to 1 (spherical particle motion). For the 'C' method, this is calculated on the waveforms after they have been corrected for splitting; we define an upper threshold and higher values are not linear enough to be considered reliable splitting measurements. With the 'O' method, the linearity is calculated on the original uncorrected waveforms; we define a lower limit, below which the particle motion is too linear to suggest splitting has occurred.

Using the suggested parameters, reliable measurements should trigger no QC flags and account for only 2 per cent of all attempted splitting measurements in this study. Measurements that fail the 'O' test but not the 'A' and 'C' tests are possible null measurements. These still provide valuable information when trying to interpret anisotropy; they should occur parallel to the fast and slow polarization directions from other splitting measurements at a station, if anisotropy is present, or they should occur for all backazimuths in the absence of anisotropy beneath the station. The measurements failing 'L' and 'T' tests can also be associated with null measurements as this occurs when there is little energy on the transverse component to constrain δt values.

4 RESULTS

Results from each station were classified as either good (A) or inadequate for interpretation (B), based on both the number and azimuthal distribution of results, as shown in Table 2. This is a subjective process, based on visual inspection of individual measurements for clarity and consistency between measurements of similar backazimuths. In our automated data, 15 stations returned good results and 19 return inadequate results. In our 10 stations with manual measurements, 6 recorded good results (a) and 4 returned inadequate results (b), with general agreement between good and inadequate stations in manual and automated data sets.

Splitting results for stations with good data are shown graphically in Figs 5 and 6 for the eigenvalue and transverse-component

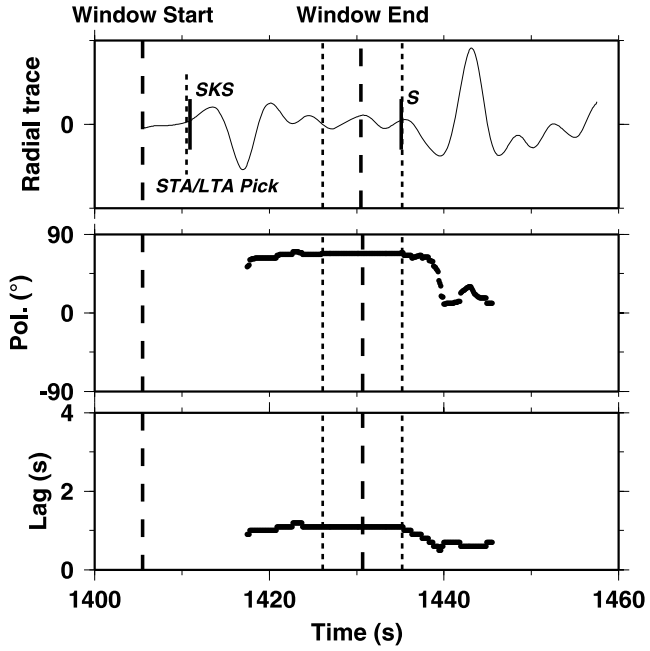

Figure 4. An example of window selection around the *SKS* arrival. The top plot shows the filtered radial waveform, with predicted arrival times for *SKS* and S phases marked as short solid lines. The short dotted line represents the pick made by the STA/LTA picking algorithm. The middle and bottom plots show variations in ϕ and δt measurements, respectively, with window length. The longest sequence of measurements over which ϕ and δt remain constant are marked by dotted lines on all three plots. The centre of this sequence is the chosen window end, marked by a dashed line. The window start, defined as 5 s before the STA/LTA pick is also defined on all three plots as a dashed vertical line.

methods, respectively, and average values are listed in Table 2. When calculating these averages, obvious outliers were excluded. Our automated results in general match well with manual measurements, which is evidence that our automated procedures work, although the automated data appears to be more scattered (see Fig. 7 for an example). However, there are significant differences between results using the eigenvalue and transverse-component methods at some stations, the clearest example being WALA (see Fig. 7), but this effect is also apparent at EDM, FRB, YKW3 and YKW4. We are confident these differences are not errors in our code or methodology as they do not occur at every station and the results have been verified using three sets of independently written software. In each case single layer interpretations seem sufficient to explain eigenvalue splitting measurements, while more complex anisotropy is suggested using the transverse energy method. At ALE, DAWY, FFC, PGC, RES, SADO, YKW1 and YKW2 simple one-layer anisotropy models fit the results from both methods.

Station INK shows two separate clusters of results, both of which contain convincing splitting measurements and so both results are included in Table 2. We suggest this may be due to multiple layers of anisotropy or lateral variations in anisotropy, but the restricted distribution of data prevents further interpretation. Similarly at FCC there appears to be a variation in splitting measurements with back-azimuth, which suggests either multiple layers or dipping anisotropy but there are insufficient clear measurements to constrain these models with any confidence.

Our results are compared with those previously published in Table 3. All differences in average ϕ are $\leq 8^{\circ}$, and only drift towards this upper limit when the numbers of data used by other researchers are comparatively small (five or less measurements). Lag time values do not match as well as polarization angle values. Some differences approach 0.6 s, but only at stations where our results suggest complex anisotropy, so the validity of such comparisons is questionable. We were unable to find published results that used the eigenvalue method for stations in this study.

Where differences between measurement methods occur we choose to use the eigenvalue derived results in our interpretation for the following reasons. Firstly, in our examples the eigenvalue results tend to require simpler anisotropy models, that tend to match well with the tectonic structures and/or absolute plate motion (APM) directions (see interpretation below). Secondly there is good correlation between eigenvalue results at YKW3 and YKW4 and those calculated using both methods at YKW1 and YKW2, which in turn match previously published results discussed above. Considering the proximity of all four stations (from 9 to 15 km), we find these differences hard to explain geologically and suggest some other factor such as misalignment of the station horizontal components may be responsible, which is investigated in more detail below.

Table 1. Quality control methods used in this study.

Method	Code	Suggested Value	Description
Polarization angle error	A	15	Maximum error accepted in polarisation angle, using either error estimation method described in the text
Lag time error	L	1	Maximum error accepted in lag value, using either error method described in the text
Maximum lag time	T	4	Maximum lag value accepted in results
Minimum eigenvalue ratio (Original traces)	O	0.05	Ratio of eigenvalues (min/max), calculated from original traces
Maximum eigenvalue ratio (Corrected traces)	C	0.03	Ratio of eigenvalues (min/max), calculated from corrected traces

The 'A' and 'L' methods define upper limits for error values defined for ϕ and δt, respectively. The 'T' method defines a maximum lag value considered realistic for splitting measurements. The 'O' and 'C' methods are calculated from the ratio of eigenvalues in the covariance matrix. The 'O' method defines a limit beneath which original traces are considered too linear to suggest splitting has occurred. The 'C' method defines an upper limit above which corrected particle motion is insufficiently linear to provide a reliable measurement.

Table 2. Results at each station.

Station	Open Date	Requests	Picks	Pick Ratio (per cent)	Eigenvalue Results	Transverse Results	Result Quality[1]	Eigenvalue		Transverse	
								Auto	Man	Auto	Man
ALE	1990-02	795	206	25.9	10	14	A	82, 1.25	–	66, 0.94	–
BBB	1993-10	594	91	15.3	2	2	B+b	–	*57, 0.95*		*50, 1.75*
BMBC	1998-01	356	72	20.2	4	7	B	*28, 1.2*	–	*25, 1.1*	–
CBB	2000-07	119	10	8.4	1	0	B	*18, 1.4*	–	*23, 1.3*	–
DAWY	1993-07	510	173	33.9	16	20	A+a	−58, 1.35	−57, 1.62	−56, 1.14	−60, 1.45
DLBC	1994-09	507	113	22.3	3	4	B+b	*−2, 0.9*	*24, 1.70*	*2, 1.0*	–
DRLN	1993-12	640	40	6.3	2	1	B	*No suitable results*			
EDM	1992-06	954	186	19.5	35	36	A+a	55, 1.15	53, 0.95	36, 1.21∗	32, 0.85∗
FCC	1993-10	896	145	16.2	9	13	A	55, 1.08∗	–	55, 0.81∗	–
FFC	1993-08	812	207	25.5	22	21	A	47, 1.08	–	40, 0.92	–
FRB	1992-06	985	143	14.5	15	31	A	−87, 0.75	–	72, 0.89∗	–
GAC	1992-05	786	48	6.1	3	1	B	*No suitable results*			
HNB	2000-11	98	13	13.3	1	1	B	*No suitable results*			
INK	1992-06	774	343	44.3	7	11	A+a	−63, 1.01∗	–	−70, 0.83∗	–
INK[2]					4	7	A+a	76, 0.73∗	–	44, 0.82∗	–
KAPO	1998-01	446	55	12.3	1	2	B	*No suitable results*			
LLLB	1998-11	279	54	19.4	0	0	B	*No suitable results*			
LMN	1993-07	768	36	4.7	6	7	B	83, 1.48	–	78, 1.3,	–
LMQ	1992-06	888	80	9.0	6	5	B	*87, 1.3*	–	*83, 1.1*	–
MOBC	1996-02	320	22	6.9	2	2	B	*No suitable results*			
OZB	1996-03	300	20	6.7	0	1	B	*No suitable results*			
PHC	2000-03	139	10	7.2	0	1	B	*52, 1.6*	–	*55, 1.7*	–
PGC	1994-07	584	91	15.8	12	16	A+a	77, 1.49	74, 1.48	77, 1.25	75, 1.44
PNT	2001-04	64	15	23.4	4	5	B	*53, 1.2*	*53, 1.20*	*-8, 1.1*	*51, 1.25*
RES	1992-06	904	203	22.5	27	31	A+a	−58, 1.40	−61, 1.64	−57, 1.23	−63, 1.45
SADO	1994-07	791	111	14.0	22	11	A	−65, 1.12	–	−88, 0.96	–
SHB	2000-11	90	9	10.0	0	0	B	*No suitable results*			
SLEB	1997-12	386	82	21.2	4	5	B	*−6, 1.3*	–	*5, 1.3*	–
SNB	2000-05	146	11	7.5	1	1	B	*−78, 0.6*	–	*−37, 0.8*	–
WALA	1992-06	944	255	27.0	44	36	A+a	64, 1.18	62, 1.07	31, 1.55∗	31, 1.43∗
WHY	1993-08	506	117	23.1	5	7	B+b	*3, 1.0*	*−4, 1.25*	*3, 1.0*	*−4, 1.25*
YKW1	1989-01	1163	412	35.4	44	51	A	44, 1.10	–	45, 1.06	–
YKW2	1989-01	1170	404	34.5	41	60	A	51, 1.13	–	50, 1.24	–
YKW3	1989-01	1158	357	30.8	39	49	A+a	47, 1.22	48, 1.37	38, 1.37∗	40, 1.56∗
YKW4	1989-01	1121	323	28.8	28	22	A	48, 1.08	–	36, 1.09∗	–
TOTALS	–	20993	4457	21.2	427	488	–	–	–	–	–

[1]Result quality abbreviated as A: Good automated results; B: Insufficient automated results for interpretation; a: Good manual results; b: Insufficient manual results for interpretation. [2]Two clusters of measurements were noticed at INK, both with convincing splitting measurements, so both are reported in this table. ∗ Indicates results suggest complex (multilayer or dipping) anisotropy models. Results in italics are those derived from a single measurement described in the text.

For stations that return inadequate results, where possible we have selected individual splitting measurements based on our subjective assessment of the available data, shown in Table 2 as values in italics. Measurements were selected on the basis of the corrected eigenvalue ratio ('C' method), the ratio of 'O' to 'C' values (in essence a measure of how much 'more linear' the solution is than the original traces) and manual inspection of the results. Note that this process is entirely subjective, but does give us the best estimates to use at stations where more thorough analysis is not possible with this data.

There are several reasons why stations may return inadequate results. Firstly, the performance of the STA/LTA picker may be poor, which may be attributable to noisy recording conditions. Secondly, the station may have been operating for an insufficient length of time. Thirdly, there may be no detectable anisotropy, a null station. This final case can be verified by the presence of null measurements across a range of backazimuths.

There are a few potential null stations in our data, the best example being LLLB (see values in Table 2). The STA/LTA picker made a sufficient number of picks on a reasonably large number of waveforms but no reliable data was found using either of the two measurement methods across a range of backazimuths.

In total 21.3 per cent of waveforms triggered the STA/LTA picker, although performance does vary considerably between stations, ranging from below 5 per cent to over 40 per cent. Only 9 per cent of these passed our QC procedures, representing less than 2 per cent of the initial data. Larger numbers of results and, therefore, better data sets are limited to stations for which at least 7 years of data were available.

5 EFFECT OF COMPONENT MISALIGNMENT ON SPLITTING MEASUREMENTS

In order to test the effects of horizontal component misalignment on shear wave splitting measurements we have adopted a method similar to that of Silver & Savage (1994). One cycle of an 8 s period sinusoid padded with Gaussian noise is used as a synthetic

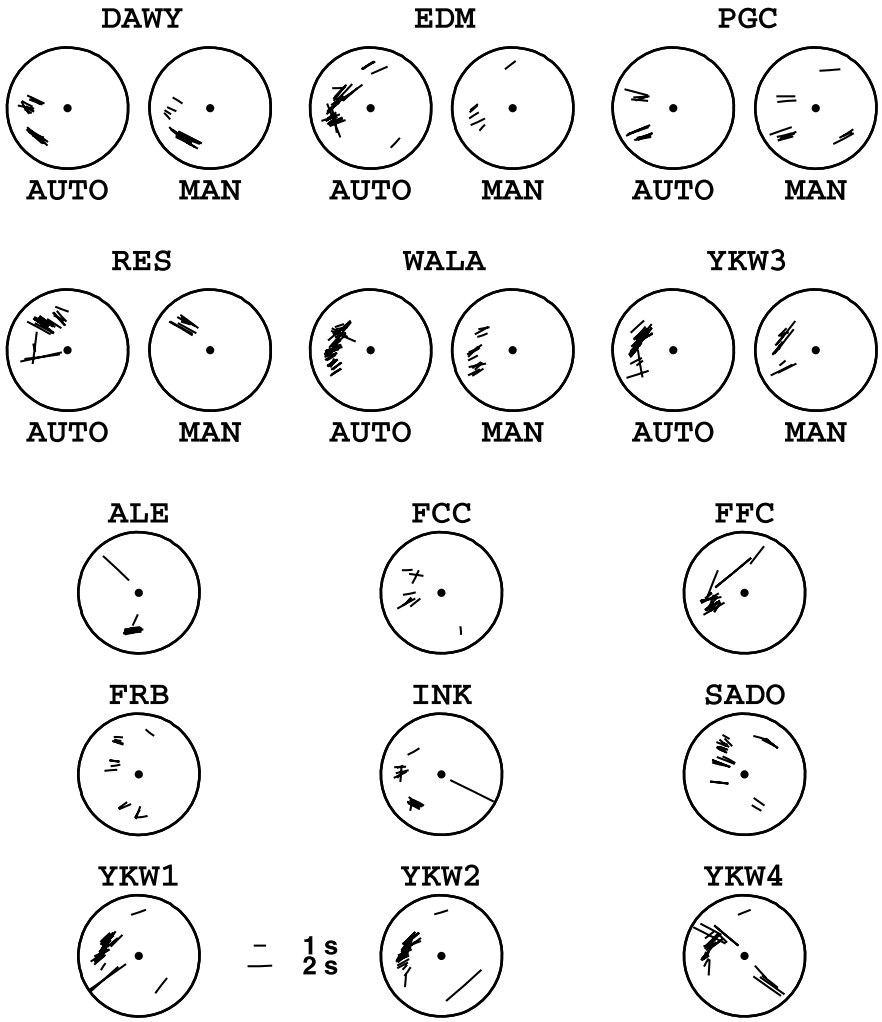

Figure 5. Eigenvalue method results for all stations with good data. Backazimuth and incidence angles are plotted on polar co-ordinates, with line orientation and length representing ϕ and δt, respectively. The top six stations have both manual and automated results, the bottom nine automated measurements only. Simple one-layer models with horizontal principal axes should show no variation in orientation with backazimuth (see DAWY for good example).

wavelet and split with the parameters $\phi = 45^\circ$, $\delta t = 1$s. The north and east components were then rotated by θ degrees to represent misalignment. The effect on apparent splitting parameters using the two measurement methods are shown in Fig. 8. Positive values represent clockwise misalignments. For the eigenvalue method, which contains no prior assumptions as to the initial polarization of the *S* wave, this misalignment offsets all ϕ values by θ degrees while the δt value remains unaffected. However, the transverse energy method rotates the corrected wavelet into radial and transverse components, which will also have been offset from their true orientation by θ degrees. This causes errors in both ϕ and δt measurements which tend to be more extreme nearer the predicted null directions and with higher values of θ. These plots of splitting parameters against backazimuth share several characteristics with those of multiple layer anisotropy models. These include tangent shaped variations in ϕ and 90° periodicity in both ϕ and δt.

To verify whether horizontal component misalignment is responsible for the differences we see in the two measurement methods we compare the initial polarization direction of the *SKS* phases, calculated from the eigenvectors in the covariance matrix, with backazimuth, see Fig. 9, along with polarization directions of direct *P* arrivals. The mean offset from predicted values is 12° and 8°, respectively, which compares well with the 10° suggested in Fig. 8.

6 INTERPRETATION

The measured splitting parameters, and hence inferred anisotropy, can be interpreted in terms of past and present mantle processes (Silver 1996). If the crust and mantle are coupled during deformation (e.g. orogeny), upper-mantle anisotropy will parallel trends in the geological structures. On the other hand, coupling between the base of the lithosphere and the underlying asthenosphere will generate anisotropy oriented in the direction of APM. We can test to see which process is more dominant beneath the Canadian stations by comparing our results with APM directions and geological trends. However, it is important to remember some subjectivity can be introduced here, as different aged tectonic structures can have varying orientations. We calculate APM using three different models (DeMets *et al.* 1994; Kreemer *et al.* 2003; Gripp & Gordon 2002).

Our clearest data come from stations on the Interior Platform (EDM, WALA and YKW1-4). At EDM and YKW we are unable to

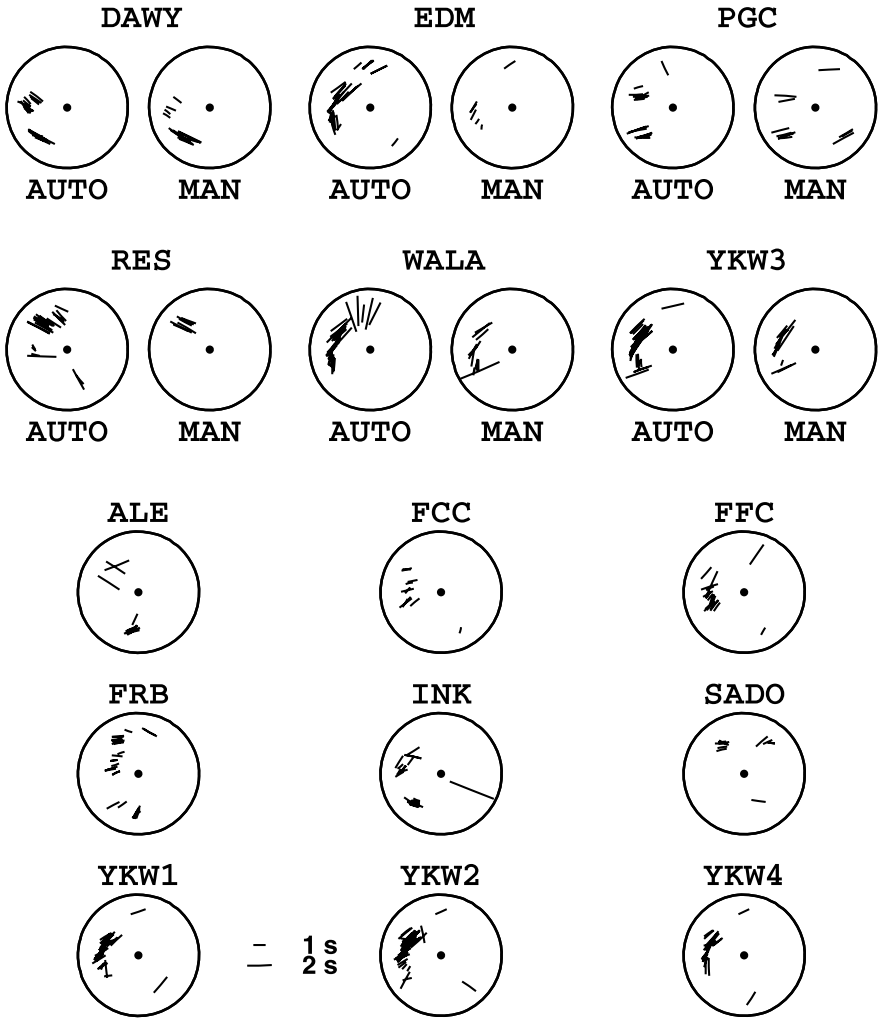

Figure 6. Transverse-component method results for stations with good data (See caption for Fig. 5 for explanation). Note the variation in orientation with backazimuth, most obvious at WALA, that was not apparent in eigenvalue method results.

distinguish between hypotheses as the orientation of tectonic features and current APM coincide and splitting parameters are parallel to both, trending NE-SW (see Fig. 10).

Further south at WALA we record similarly oriented splitting measurements, but this station is located within thrust faults associated with the Canadian Cordillera that align roughly NW–SE. This suggests APM must be the dominant process beneath this station. We see close correlation between splitting measurements and the strike of the Tintina Trench at DAWY, further north within the Canadian Cordillera. This fault effectively outlines the limits of deformation related to the orogeny, which suggests vertically coherent deformation at this station.

At PGC on Vancouver Island there is significantly better correlation between splitting measurements and the APM of the subducting Juan de Fuca plate, rather than any features related to the overriding North American plate, as is also discussed by Currie *et al.* (2004).

There is reasonable correlation between splitting measurements at ALE and nearby faults related to the Proterozoic Innuitian orogeny (Fig. 11), although the region later underwent similarly oriented compressional tectonics in the Late Cretaceous–Early Oligocene Eurekan orogeny (Aitken 1993). Both these results agree with the observations of Bostock & Cassidy (1995) and Hellfrich *et al.* (1994), respectively. There is a close correlation between measurements at LMN and the trend of structures related to the Appalachian orogeny (Fig. 12), but this result is only based on 5 measurements. Barruol & Hoffman (1999) and Levin *et al.* (1999) arrived at a similar conclusion for other Appalachian stations. There is also some correlation between splitting parameters at SADO in Ontario and the orientation of the boundary between the Grenville Province and the St. Lawrence Platform (Douglas 1973).

At other stations correlations are less clear. At FRB tectonic structures trend NW–SE, which does not correlate well with splitting measurements which align E–W. APM models at this station are closer, but there is significant disagreement between models at this station, varying from -75° to -120°. Splitting measurements at FFC are orientated NE–SW, which align better with approximately WSW APM models than the E–W faults in the area. At RES neither tectonic structures (N–S) or APM models (-104° to -146°) correlate with splitting measurements, which are clustered around -60°. Unfortunately our automated method has not returned good results from the dense network of broad-band stations in southern British Columbia due to their relatively recent deployment and, therefore, limited data. Individual splitting measurements were possible at some stations, but we suggest results from the more detailed study by Currie *et al.* (2004) are more reliable.

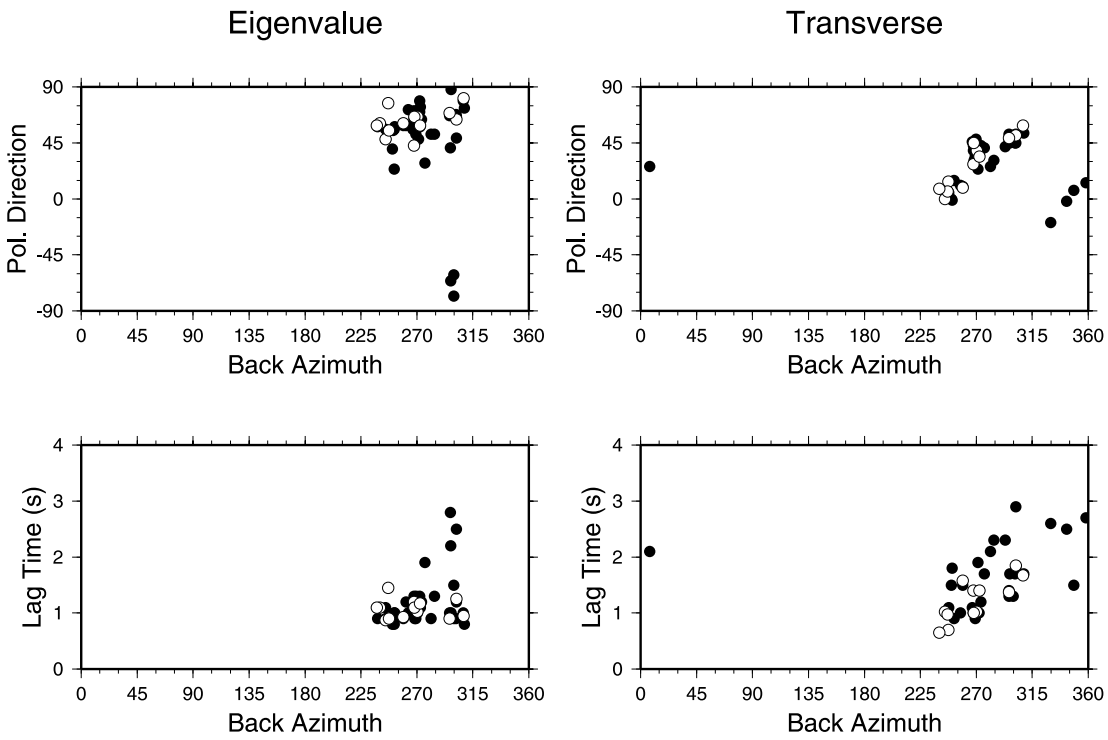

Figure 7. Example of differences between results for the eigenvalue and transverse-component method applied at station WALA. Black circles are automated measurements, open circles are manual measurements. The correlation is good between automated and manual measurements in each case, but there is poorer correlation between eigenvalue and transverse results. A simple one-layer solution fits the eigenvalue results reasonably well, but transverse-component results require a more complex model such as multiple layers of anisotropy. Note also that in both cases the automated measurements contain more statistical outliers.

Table 3. Comparison between automated results and previously published data.

Station	Method [a]	Automated results		Published results		
		Values(ϕ, δt)	No. Data	Source [b]	Values (ϕ, δt)	No. data
ALE	T	66, 0.94	14	H	61, 0.91	3
DAWY	T	−56, 1.14	20	BOS	−64, 1.35	5
EDM	T	36, 1.21*	36	BOS	33, 0.60	3
FFC	T	40, 0.92	21	BOS†	48, 0.70	–
FRB	T	72, 0.89*	31	BOS†	78, 0.70	–
PGC	T	77, 1.25	16	BOS	74, 1.15	6
				CUR	77, 1.03	12
RES	T	−57, 1.23	31	BOS†	-60, 0.95	-
WALA	T	31, 1.55*	36	BOS	37, 0.90	8
YKW2	T	50, 1.24	60	BOS	53, 1.55	3
RSNT[1]	T	–	–	S&C	51, 1.20	9

[a] All published results found used the transverse-component method (T).
[b] Sources abbreviated as H: Hellfrich *et al.* (1994); BOS: Bostock & Cassidy (1995); BOS†: Bostock & Cassidy as quoted in Silver (1996); CUR: Currie *et al.* (2004); S&C: Silver & Chan (1991).
*Complex anisotropy suggested from automated results. [1] Station RSNT is approximately 6 km from YKW2.

7 CONCLUSIONS

We have developed an automated shear wave splitting measurement method. Tests with data from seismic stations in Canada show that there is a good correlation between automated and manual results and with those of other authors. Phase onset is found using the STA/LTA picker of Earle & Shearer (1994) and the selected window size is based on the analysis of repeated measurements over progressively larger windows. Our clearest data is from stations where at least 7 years of waveform data were available. This figure is not necessarily indicative of a global average as results are dependent on local noise conditions and the distribution of natural seismicity. Only 2 per cent of all requested data passed our QC procedures, although this figure could be increased if optimum QC parameters were found for individual stations.

The effects of horizontal component misalignment on transverse energy method measurements share many characteristics with multilayer anisotropy models, including tangent shaped variations in ϕ and 90○ periodicity in both ϕ and δt. We find that the eigenvalue method is more stable under these conditions, with misalignment manifesting itself as errors in polarization direction rather than more complex anisotropy models. We suggest researchers using the transverse energy method who find results indicative of more complex anisotropy models eliminate the possibility of misalignment

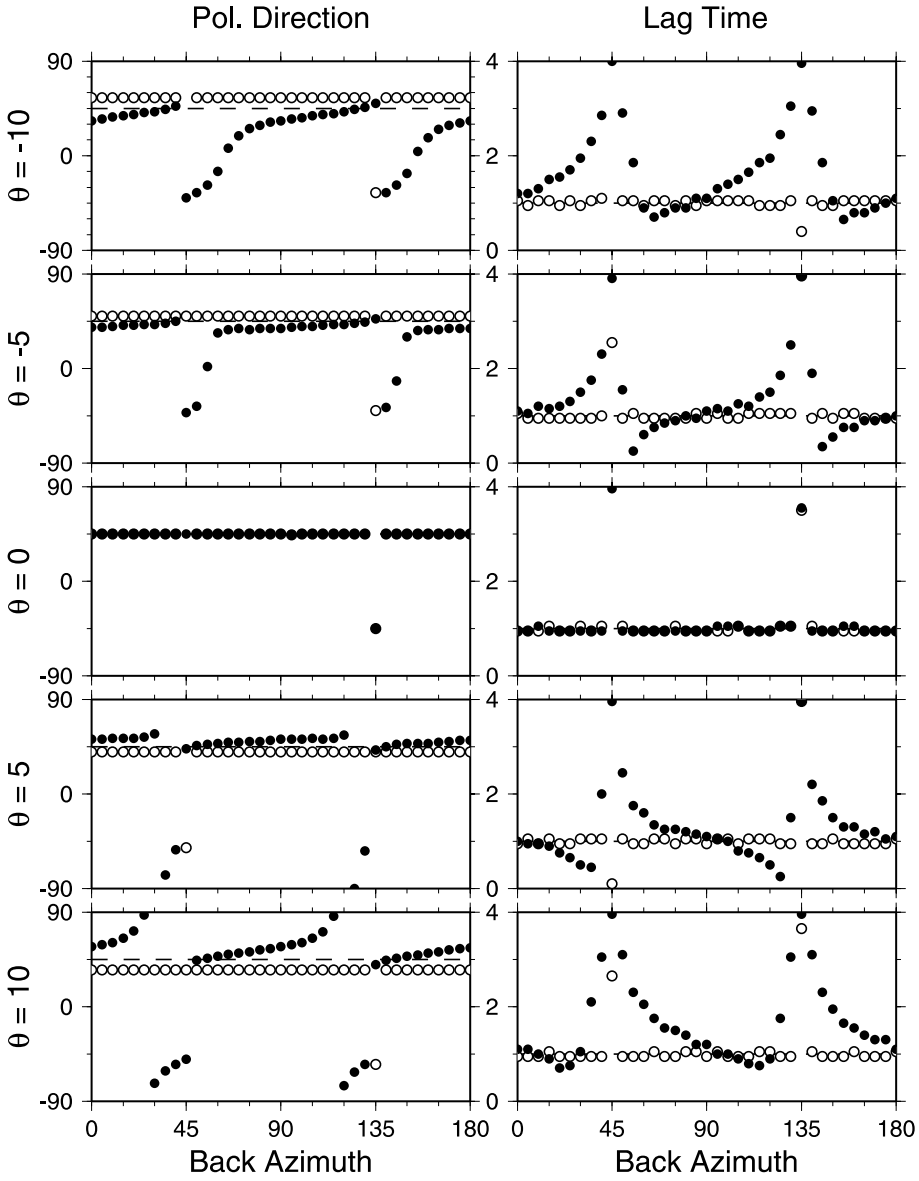

Figure 8. Splitting parameters for eigenvalue and transverse energy measurements under the circumstance of horizontal component misalignment. Each example has one anisotropic layer with the parameters $\phi = 45^\circ$, $\delta t = 1$s. Components are misaligned by $\theta = -10, -5, 0, 5$ and 10 degrees, respectively, (positive = clockwise rotation). The eigenvalue method measurements (open circles) remain constant in each plot. Negative θ values lead to an increase in ϕ by θ, except at the predicted null backazimuths (45 and 135°). The δt value remains unaffected. Transverse energy method measurements are closed circles, and vary in both ϕ and δt, except for the case where $\theta = 0$. Dashed lines show the true splitting values. Note the similarities between the top plots ($\theta = -10^\circ$) and Fig. 7.

by comparing results with eigenvalue derived measurements and/or the polarization of direct *P* arrivals.

Splitting results from Canadian stations parallel tectonic structures in the Northern Canadian Cordillera, the Innuitian orogeny and in the Appalachian orogeny. This is consistent with the hypothesis of vertically coherent deformation between the crust and mantle. At stations in central Canada, splitting measurements more closely align with APM directions than geological features, but correlation is less well defined. This could be because APM is an oversimplification, and more detailed 3-D mantle flow models may be required, (e.g. Fouch *et al.* 2000; Becker *et al.* 2003).

Our results suggest that the dominant cause of anisotropy will depend on the nature of the tectonic environment. Such conclusions should be more apparent as data from more stations are analysed, and future work involves automated analyses of *SKS* splitting at GSN stations worldwide. Splitting measurements generated in this study are available through a web interface located at http://www.isc.ac.uk/SKS and all source code used in this study are available via FTP at ftp://ftp.isc.ac.uk/pub/SKS.

ACKNOWLEDGMENTS

Many thanks to K. Walker, J. Plomerova and T. Becker for their detailed comments and suggestions, which have greatly improved this manuscript. Research of this nature would not be possible without the waveform data services offered by data centres to the wider academic community. In this study we have extensively used the AutoDRM service of Earthquakes Canada and the NetDC service

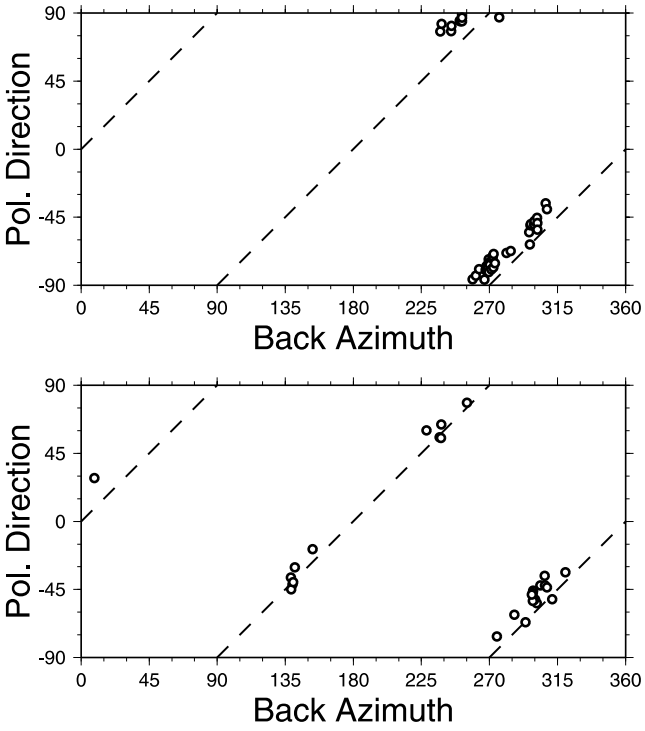

Figure 9. The top plot shows polarization directions of corrected *SKS* phases using the eigenvalue method plotted against backazimuth at WALA. The predicted backazimuth is shown by the dashed line. There is a distinct bias towards larger polarization values consistent with anticlockwise misalignment, (mean offset 12°). The bottom plot shows polarization directions of direct P arrivals measured at the same station, (mean offset 8°).

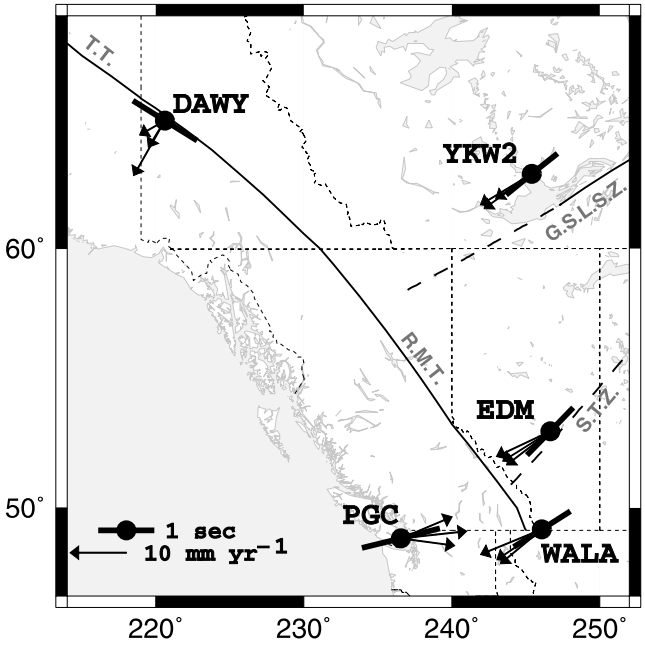

Figure 10. Correlation between splitting measurements, tectonic features and APM directions for stations in Western Canada. T.T.: Tintina Trench. R.M.T. Rocky Mountain Trench G.S.L.S.Z.: Great Slave Lake Shear Zone. S.T.Z.: Snowbird Tectonic Zone. Orientation of geological features from Hoffman (1989); Wheeler *et al.* (1991, 1996). Arrows are estimates of current day APM taken from DeMets *et al.* (1994), Kreemer *et al.* (2003) and Gripp & Gordon (2002). APM estimates for PGC are those of the subducting Juan de Fuca plate, rather than the North American plate.

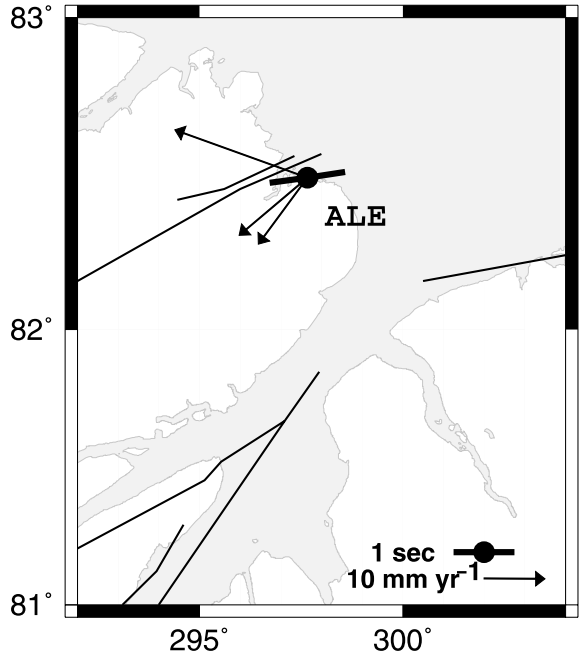

Figure 11. Splitting measurements in relation to APM and tectonics of the Innuitian orogeny. There is good correlation between splitting measurements and the trend of faults related to the Proterozoic Innuitian orogen (taken from Okulitch (1991).

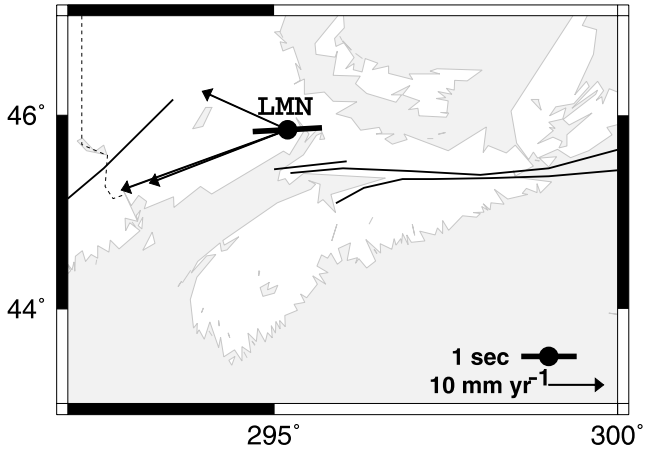

Figure 12. Splitting measurements in relation to APM and tectonics of the Appalachian orogeny. Fault trends taken from Wheeler *et al.* (1996).

of the IRIS Data Management Centre. We would also like to thank the International Seismological Centre for providing Bulletin data and the continued use of their computing facilities, and the staff of the Czech Academy of Sciences for assistance with splitting codes in the early stages of this project.

The IRIS DMS is funded through the National Science Foundation and specifically the GEO Directorate through the Instrumentation and Facilities Program of the National Science Foundation under Cooperative Agreement EAR–0004370.

Funding for this project was provided by NERC grant NER/A/S/2001/00524.

REFERENCES

Aitken, J.D., 1993. Evolutionary models and tectonic comparisons; chapter 13 in *Sedimentary Cover of the Craton of Canada*, pp. 799–808, eds Scott, D.F. & Aitken, J.D., Geological Survey of Canada, Geology of Canada no. 5.

Alsina, D. & Sneider, R.K., 1995. Small scale sublithospheric continental deformation: constraints from SKS splitting observations, *Geophys. J. Int.,* **123,** 431–448.

Ando, M. & Ishikawa, Y., 1982. Observations of shear-wave polarisation anisotropy beneath Honshu, Japan: two masses with different polarizations in the upper mantle, *J. Phys. Earth,* **30,** 191–199.

Barruol, G. & Hoffman, R., 1999. Upper mantle anisotropy beneath the GEOSCOPE stations, *J. geophys Res.,* **104,** 10 757–10 773.

Becker, T.W., Kellogg, J.B., Ekstrom, G. & O'Connell, R.J., 2002. Comparison of azimuthal seismic anisotropy from surface waves and finite strain from global mantle-circulation models, *Geophys. J. Int.,* **155,** 696–714.

Bostock, M.G. & Cassidy, J.F., 1995. Variations in SKS splitting across western Canada, *Geophys. Res. Lett.,* **22,** 5–8.

Butler, R. et al., 2004. The global seismograph network surpasses its design goal, *EOS, Trans. Am. geophys. Un.,* **85,** 225–229.

Chevrot, S., 2000. Multichannel analysis of shear wave splitting, *J. geophys Res.,* **105,** 21 579–21 590.

Currie, C.A., Cassidy, J.F., Hyndman, R.D. & Bostock, M.G., 2004. Shear wave anisotropy beneath the Cascadia subduction zone and western North America craton, *Geophys. J. Int.,* **157,** 341–353.

DeMets, C., Gordon, R.G., Argus, D.F. & Stein, S., 1994. Effect of recent revisions to the geomagnetic reversal time scale on estimates of current plate motions, *Geophys. Res. Lett.,* **21,** 2191–2194.

Douglas, R.J.W., 1973. Geological Provinces, The National Atlas of Canada, *Geological Survey of Canada*.

Earle, P.S. & Shearer, P.M., 1994. Characterization of global seismograms using an automatic picking algorithm, *Bull. seism. Soc. Am.,* **84,** 366–376.

Earthquakes Canada, 2003. GSC *Continuous Waveform Archive*, AutoDRM@seismo.NRCan.gc.ca, *Nat. Res. Can,* see: http://earthquakescanada.nrcan.gc.ca/cite_e.php.

Fouch, M.J., Fischer, K.M., Parmentier, E.M., Wysession, M.E. & Clarke, T.J., 2000. Shear wave splitting, continental keels and patterns of mantle flow, *J. geophys. Res.,* **105,** 6255–6276.

Gripp, A.E. & Gordon, R.G., 2002. Young tracks of hotspots and current plate velocities, *Geophys. J. Int.,* **150,** 321–361.

Hellfrich, G., Silver, P. & Given, H., 1994. Shear-wave splitting variations over short spatial scales on continents, *Geophys. J. Int.,* **119,** 561–573.

Hoffman, P.F., 1989. Precambrian geology and tectonic history of North America in *The geology of North America—an overvew*, eds Bally, A.W. & Palmer, A.R., Geological Society of North America.

International Seismological Centre, 2003. On-line Bulletin, *http://www.isc.ac.uk/Bull*, Internatl. Seis. Cent., Thatcham, UK.

Kennett, B.L.N. & Engdahl, E.R., 1991. Traveltimes for global earthquake location and phase identification, *Geophys. J. Int.,* **105,** 429–465.

Kreemer, C., Holt, W.E. & Haines, A.J., 2003. An integrated global model of present day plate motions and plate boundary deformation, *Geophys. J. Int.,* **154,** 8–34.

Levander, A., Humpreys, G., Ekstrom, G., Meltzer, A. & Shearer, P., 1999. USArray: An earth sciences initiative to investigate the North American continent *EOS Trans AGU.,* **80,** 245.

Levin, V., Menke, W. & Park, J., 1999. Shear wave splitting in the Appalachians and the Urals: A case for multilayered anisotropy, *J. geophys. Res.,* **104,** 17 975–17 993.

Okulitch, A.V., 1991. Geology of the Canadian archipelago and north Greenland; *Figure 2 in Innuitian orogen and Arctic platform: Canada and Greenland*, ed. Trettin, H.P., Geological Survey of Canada.

Plomerova, J., Sileny, J. & Babuska, V., 1996. Joint interpretation of upper-mantle anistropy based on teleseismic P-travel time delays and inversion of shear-wave splitting parameters, *Phys. Earth planet. Int.,* **95,** 293–309.

Sandvol, E. & Hearn, T., 1994. Bootstrapping shear-wave splitting errors, *Bull. seism. Soc. Am.,* **84,** 1971–1977.

Savage, M.K. & Silver, P.G., 1993. Mantle deformation and tectonics: constraints from seismic anisotropy in Western United States, *Phys. Earth planet. Int.,* **78,** 207–227.

Sileny, J. & Plomerova, J., 1996. Inversion of shear-wave splitting parameters to retrieve three-dimensional orientation of anisotropy in continental lithosphere, *Phys. Earth planet. Int.,* **95,** 277–292.

Silver, P.G., 1996. Seismic anisotropy beneath the continents: Probing the depths of geology, *Annu. Rev. Earth Pl. Sc.,* **24,** 385–432.

Silver, P.G. & Chan, W.W.J., 1991. Shear-wave splitting and subcontinental mantle deformation, *J. geophys. Res.,* **96,** 16 429–16 454.

Silver, P.G. & Savage, M.K., 1994. The interpretation of shear-wave splitting parameters in the presence of two anisotropic layers, *Geophys. J. Int.,* **119,** 949–963.

Vinnik, L.P., Kosarev, G.L. & Makeyeva, L.I., 1984. Anisotropy of the lithosphere according to the observations of SKS and SKKS waves, *Dokl. Akad. Nauk. SSSR.,* **278,** 1335.

Vinnik, L.P., Farra, V. & Romanowicz, B., 1989. Azimuthal anisotropy in the earth from observations of SKS at GEOSCOPE and NARS broadband stations, *Bull. seis. Soc. Am.,* **79,** 1542–1558.

Wheeler, J.O., Brookfield, A.J., Gabrielse, H., Monger, J.W.H., Tipper, H.W. & Woodsworth, G.J., 1991. Terrane map of the Canadian Cordillera, *Geological Survey of Canada.*, Map 1713A.

Wheeler, J.O., Hoffman, P.F., Card, K.D., Davidson, A., Sanford, B.V., Okulitch, A.V. & Roest, W.R., 1996. Geological Map of Canada, *Geological Survey of Canada.*, Map 1860A.

Wookey, J., Kendall, J.-M. & Rumpker, G., 2005. Lowermost mantle anisotropy beneath the north Pacific from differential S-ScS splitting, *Geophys. J. Int.* **161,** 829–838.